Paper No.
2149

Investigation of Pseudo-Passivation of Mild Steel in CO_2 Corrosion

Wei Li, Bruce Brown, David Young and Srdjan Nesic
Institute for Corrosion and Multiphase Technology
Department of Chemical & Biomolecular Engineering
Ohio University
342 West State St., Athens, OH 45701
United States

ABSTRACT

The iron carbonate corrosion product layer formed on mild steel in CO_2 environments is known to retard corrosion. When not fully covering the steel surface, it may also lead to initiation of localized corrosion, due to a galvanic effect. In this work, the stability of a protective iron carbonate layer has been studied at 80°C over a relatively wide range of bulk pH. Experiments were done in a glass cell using a three electrode system. Electrochemical techniques such as linear polarization resistance (LPR) and electrochemical impedance spectroscopy (EIS) were used. Surface analysis techniques (SEM, XRD, TEM) were employed to confirm the composition and structure of the protective layer. Experimental results confirmed a pseudo-passive behavior, indicated by a positive shift in the open circuit potential and a significantly retarded corrosion rate for systems at pH 6.0 and above. However, a stable and protective pseudo-passive layer could not be formed at pH 5.6 or lower.

Keywords: CO_2 corrosion product layer, pseudo-passivation, electrochemical techniques, SEM, XRD, TEM.

INTRODUCTION

Internal CO_2 corrosion problems are common in the oil and gas industry. This is due to the fact that carbon steel is the primary structural material for transportation pipelines and the aqueous CO_2 environment within the lines has the potential to be corrosive. Although carbon steel has a low cost and a relatively high strength, its corrosion resistance is limited. Use of pH control to provide a more neutral environment and stimulate formation of protective corrosion product layers may leave carbon steel more vulnerable to localized corrosion attack[1]. Despite the fact that the general CO_2 corrosion mechanisms are well understood[2-5], the role of the protective corrosion product layer and its potential to lead to localized CO_2 corrosion remains unclear.

$FeCO_3$ is a common CO_2 corrosion product found on internal surfaces of mild steel pipelines. As long as Fe^{2+} and CO_3^{2-} are present in the brine at sufficiently high concentrations which exceed saturation with respect to $FeCO_3$, precipitation and crystal growth will occur[6], according to:

$$Fe^{2+}(aq.) + CO_3^{2-}(aq.) \rightarrow FeCO_3(s.) \quad (1)$$

The important threshold is the $FeCO_3$ saturation value (S), calculated by:

$$S_{(FeCO_3)} = \frac{C_{Fe^{2+}} \times C_{CO_3^{2-}}}{K_{sp}} \quad (2)$$

Based on Equation (2) a graph showing the relationship between $C_{Fe^{2+}}$, pH and $S_{(FeCO3)}$ can be constructed (see Figure 1). A strong dependency of $S_{(FeCO3)}$ on $C_{Fe^{2+}}$ and pH is apparent. The water chemistry and equilibrium constants that are used for constructing this chart were derived from the literature[7-11]. In Figure 1, the line which has a $S_{(FeCO3)}$ of 1 divides the field into two zones: $FeCO_3$ supersaturated and $FeCO_3$ undersaturated regions. In the $FeCO_3$ supersaturated region ($S_{(FeCO3)}$ > 1), according to Equation (2), there is an excess of Fe^{2+} and CO_3^{2-}. Hence, the $FeCO_3$ precipitation process is assumed to prevail over the simultaneously occurring $FeCO_3$ dissolution (as given by Equation 1). In this case a $FeCO_3$ layer is expected to develop on the steel surface. Conversely, in the $FeCO_3$ undersaturated region ($S_{(FeCO3)}$ < 1), the rate of $FeCO_3$ dissolution process is faster than the rate of $FeCO_3$ precipitation and an $FeCO_3$ layer cannot form. In Figure 1, two dotted lines representing the saturation value of 0.5 and 2 are plotted adjacent to the saturation line. The region between the dotted lines is considered an unstable region for $FeCO_3$ development and named the "gray zone". In this area, $FeCO_3$ is either slightly supersaturated or undersaturated, a scenario where precipitation and dissolution processes closely compete with each other. Hence, no single process is dominant, which could lead to the metal surface being partially covered by $FeCO_3$ and a possibility of localized corrosion.

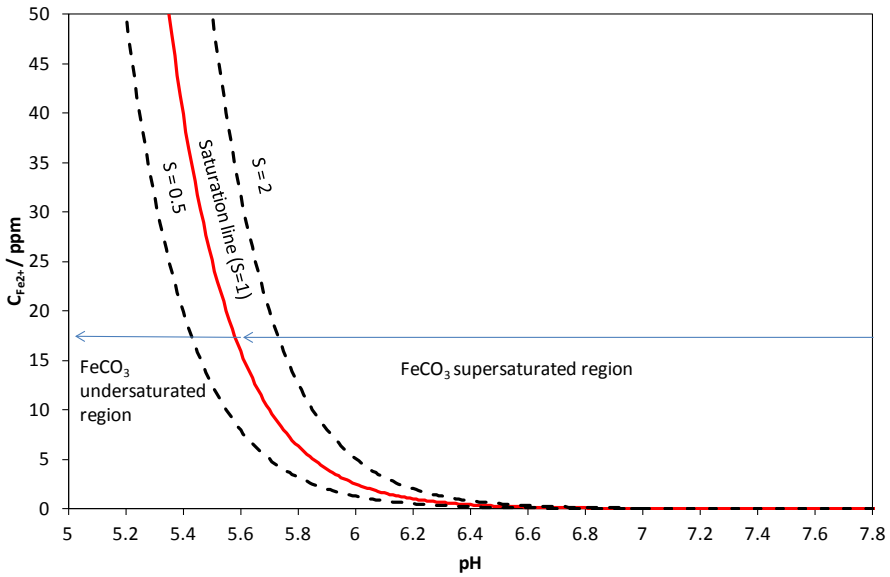

Figure 1: Calculation of the dependency of $FeCO_3$ solubility on $C_{Fe^{2+}}$ and pH (80°C, pCO_2 = 0.53 bar(53 kPa), 1 wt.% NaCl).

It has been commonly accepted that the $FeCO_3$ layer is protective because it presents a mass transfer barrier and slows down the diffusion of cathodic species to the steel surface. However, the effect of direct steel surface coverage, blocking the anodic dissolution of iron, seems to be just as important. Han, *et al.*[12], observed a significant increase of open circuit potential accompanied with a dramatic decrease in corrosion rate when the metal surface was covered by a $FeCO_3$ layer – a behavior they termed *pseudo-passivation*. The pH is a critical factor which affects pseudo-passivation. High pH promotes formation of a protective $FeCO_3$ layer and pseudo-passivation. Conversely, a decrease in pH will readily lead to a loss of protection.

The influencing factors in developing a pseudo-passive CO_2 corrosion product layer are not fully understood[13]. Han, *et al.*[12] focused primarily on very high pH (pH>6.6) in an effort to cause pseudo-passivation to occur more rapidly. Very few tests of pseudo-passivation were done in the lower pH range, *i.e.*, at conditions which are more commonly observed in upstream pipelines for oil and gas transportation. In the present study, the stability of a pseudo-passive layer over a broader pH range is investigated. Questions about the mechanism of the formation of this layer, as well as its morphology and chemical composition, will be addressed in this paper.

EXPERIMENTAL

A 2 liter glass cell was used for the experiments. The schematic is shown in Figure 2. A three-electrode system was employed for electrochemical measurements. Ag/AgCl and platinum wire were selected as the reference electrode (RE) and counter electrode (CE), respectively. A cylindrical mild steel specimen (outer diameter 12.0mm; length 14.4mm) was used as the working electrode (WE). Additional flat specimens (1.0 cm x 1.0 cm x 0.2 cm) were independently suspended by nylon string in the glass for retrieval during the test in order to do *ex situ* surface analyses. Images of these specimens are shown in Figure 3.

Electrochemical measurements using open circuit potential (OCP) and linear polarization resistance (LPR) were conducted systematically with a potentiostat (Gamry† Reference 600).The detailed parameter selections of the electrochemical measurements are listed in Table 1. An increase in OCP that occurs concurrently with a corrosion rate decrease is considered a distinctive indication of a pseudo-passive layer formation[12]. Therefore, OCP and corrosion rate were monitored continuously during the tests.

Ferrous ion concentration $C_{Fe^{2+}}$, in the glass cell was measured *ex-situ* by a UV/Vis spectrophotometer and used to calculate the $FeCO_3$ saturation value $S_{(FeCO3)}$ in the system. Scanning electron microscopy (SEM), X-ray diffraction (XRD), grazing incidence X-ray diffraction (GIXRD) and transmission electron microscopy (TEM) were employed for sample surface analyses.

The focus of this study was how pH affects the formation of a protective pseudo-passive layer. Consequently, test systems with different pH values were investigated; the test matrix is shown below (Table 2). It should be noted that, in the lower pH range, $FeCO_3$ is undersaturated (see Figure 1). In order to control the $FeCO_3$ saturation value, $S_{(FeCO3)}$, a deaerated $FeCl_2$ solution was syringe injected into the test system to increase the ferrous ion concentration, $C_{Fe^{2+}}$.

Before each test, a 1 wt.% NaCl solution was prepared in the glass cell reactor, deaerated with a continuous CO_2 gas flow purge and heated to the test temperature by a hot plate. After the designated temperature was achieved, the bulk pH was adjusted by addition of $NaHCO_3$, Na_2CO_3 or dilute HCl solution (0.1M). Both of the cylindrical and flat samples were evenly polished by sand paper with 400 and 600 grit numbers, sequentially, and then cleaned in an ultrasonic bath with isopropanol. Samples then were taken out and dried by nitrogen gas and immediately used for testing.

† Trade Name

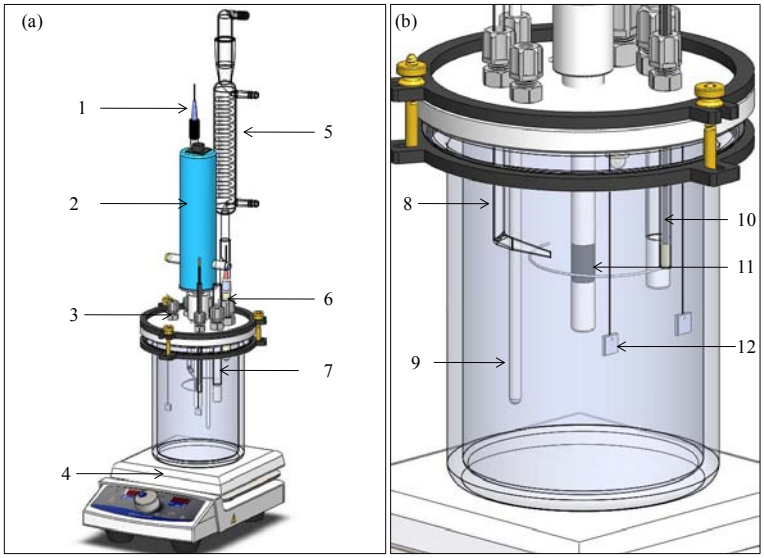

Figure 2: (a) Schematic of glass cell setup; (b) enlarged view of glass cell
(courtesy of Cody Shafer, research engineer, ICMT, Ohio University)

1. Reference electrode	2. Rotator motor	3. Gas outlet
4. Hot plate	5. Condenser	6. pH probe
7. Gas inlet tubing	8. Luggin capillary	9. Temperature probe
10. Counter electrode	11. Cylindrical working electrode	12. Flat specimen

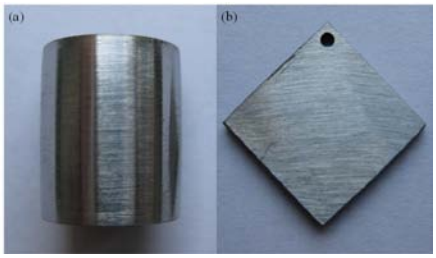

Figure 3: Pictures of (a) cylindrical WE and (b) flat specimen, both made from (API[(1)] 5L X65).

[(1)] American Petroleum Institute (API), 1220 L Street, NW, Washington, DC 20005-4070

Table 1. Parameter selections of electrochemical measurements

Technique	Parameters
LPR	Scan Rate: 0.1 mV / s. Sample Period: 1s. Polarization range: ± 5 mV (*vs.* EOC). Resolution: 0.125 mV B value: 26 mV

Table 2. Test matrix for protective iron carbonate layer study in CO_2 corrosion system

pH	7.8	7.1	6.6	6.0	5.6
Test material	X-65 carbon steel				
Temperature (^oC)	80				
Supporting electrolyte	1 wt.% NaCl				
CO_2 partial pressure	0.53				
Initial $C_{Fe^{2+}}$ (ppm)	0	0	50	100	1000

When the samples were removed from the system after test completion, unwanted corrosion product layer oxidation may occur due to exposure to air, and affect the subsequent surface analyses. In order to minimize this effect, samples were immediately dehydrated and stored in vacuum desiccators.

RESULTS AND DISCUSSION

Effect of pH on protective corrosion product layer

As indicated in Figure 1, the pH can significantly influence the saturation state of $FeCO_3$, which consequently influences the formation of protective corrosion product layers. Figure 4 shows the open circuit potential and the corrosion rate for tests at different pH values. For bulk pH values above 7.0 (high pH), from Figure 4 (a) and (b), a significant OCP increase (more than 200 mV) can be observed. At the same time, the corrosion rate is low and stable (less than 0.01 mm/yr). This clearly shows that for bulk pH values above 7.0, a stable, protective pseudo-passive layer has formed in a spontaneous corrosion process without any addition of excess ferrous ions in solution. This can be easily explained by looking at the dependency of $FeCO_3$ solubility on $C_{Fe^{2+}}$. and pH (Figure 1). For these pH values, conditions are such that saturation with respect to $FeCO_3$ is reached even at very low $C_{Fe^{2+}}$ and the solution will readily become supersaturated due to corrosion. A well-developed $FeCO_3$ layer is expected to form under these conditions and cover the entire carbon steel surface, offering good corrosion protection. Corrosion product layer characterization was done to confirm this and will be discussed in the following section.

For tests at bulk pH 6.6 and 6.0, the formation of a pseudo-passive layer is also indicated in Figure 4 (c) and (d). However, the degree of protectiveness is somewhat lower than for the higher pH tests. A noticeable OCP increase, less than 100 mV, can still be seen; and the final corrosion rate is low, around 0.1 mm/yr. In this bulk pH range, the conditions are undersaturated with respect to $FeCO_3$ formation (without additional ferrous ions present in solution). Therefore, a calculated amount of ferrous chloride was added to the test system to achieve supersaturation and stimulate $FeCO_3$ precipitation from the bulk solution. It is also necessary to note that the time to form a protective layer in this pH range is longer than for the tests above pH 7. In the pH range of 6.6 to 6.0, it takes more than 3 days before the corrosion rate reaches a low value. However, for the higher pH tests, the corrosion rate is low after only 1 day.

The test at bulk pH 5.6 (Figure 4 (e)) shows that pseudo-passivation could not be achieved. Neither an OCP increase nor a significant corrosion rate decline can be seen after an extended period (22 days). Considering the fact that the $FeCO_3$ is significantly undersaturated at this test condition, two large additions of ferrous chloride were made at the 1st and the 13th day of this test (1000 ppm and 1400 ppm, respectively) in order to achieve a high $FeCO_3$ saturation value. This elevated ferrous ion concentration did initiate precipitation and formation of a corrosion product layer over a period of time (from day 6 to day 18). However, ferrous ions were depleted in the solution due to the precipitation of $FeCO_3$ and the pH decreased in the process. Eventually, corrosion prevailed and the effect of induced $FeCO_3$ precipitation vanished.

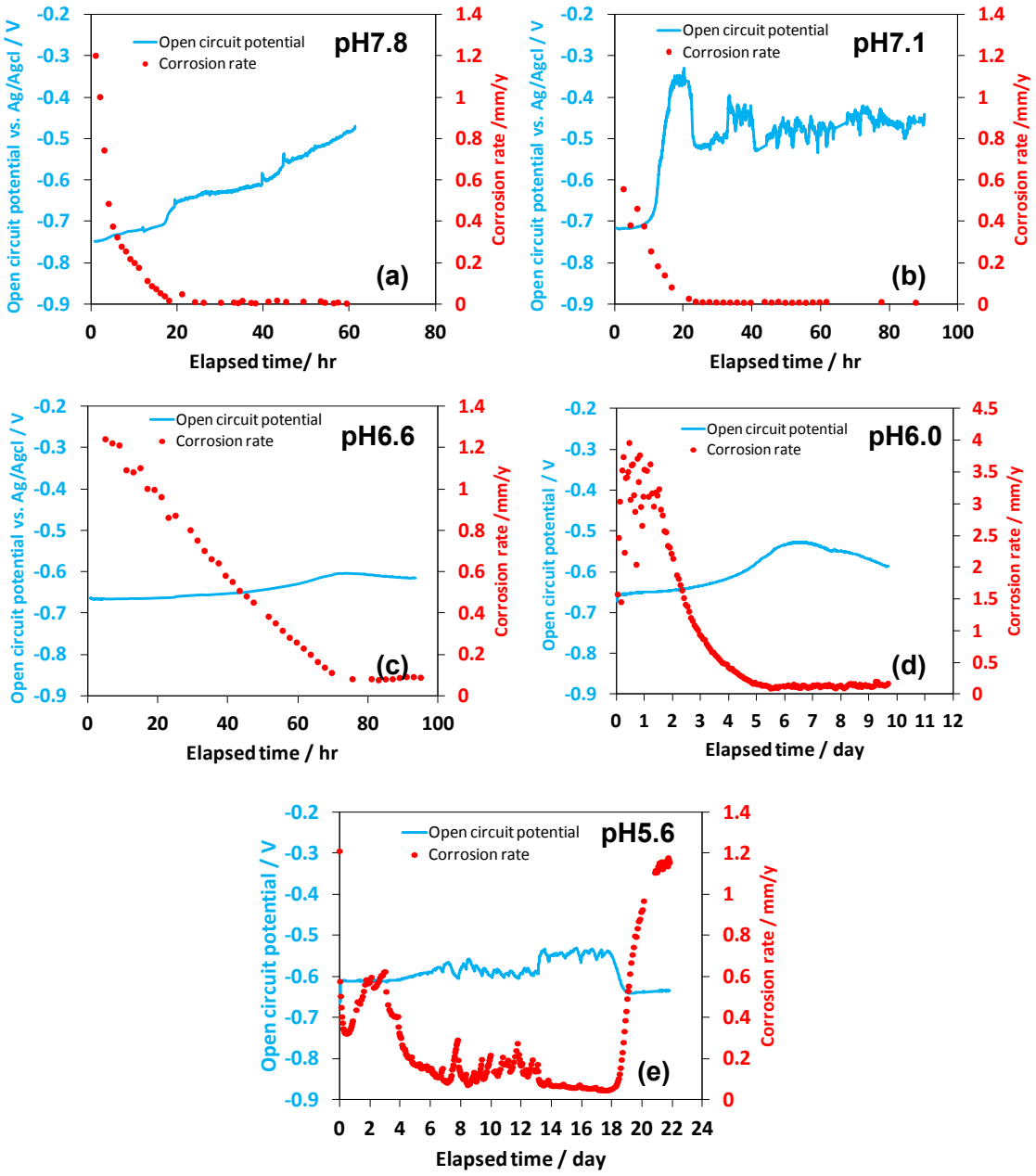

Figure 4: Variations of open circuit potential and corrosion rate with time at different pH (80°C, 0.53 bar (53 kPa) CO_2, 1 wt.% NaCl, stagnant): (a) pH 7.8; (b) pH 7.1; (c) pH 6.6, initial $C_{Fe^{2+}}$= 50 ppm; (d) pH 6.0, initial $C_{Fe^{2+}}$= 100 ppm; (e) pH 5.6, initial $C_{Fe^{2+}}$= 1000 ppm, second $C_{Fe^{2+}}$addition at the 13th day to 1400 ppm. For corresponding SEM images see Figure 5.

Morphology and composition of the corrosion product layers

In Figure 5, SEM images of the samples after each test are shown. They clearly show transitions in surface morphology due to the bulk pH change. At high pH (pH 7.8 and pH 7.1), the $FeCO_3$ prism-shaped crystals cover the entire sample surface. At the intermediate pH values (pH 6.6 and pH 6.0), the dominant morphology of $FeCO_3$ becomes platelets, which would imply a less densely packed, and more polycrystalline corrosion product layer structure. A few prism-shaped $FeCO_3$ crystals are observed. At the low pH value tested (pH 5.6), the steel surface was barely covered with any prismatic $FeCO_3$. In each case the main component of this layer was determined by XRD to be $FeCO_3$.

The dense prism-shaped $FeCO_3$ crystals packing on the steel surface at pH 7.8 (Figure 5a) offers good corrosion protection (see Figure 4a). It seems plausible to assume that this is because the dense $FeCO_3$ layer acts as a mass transfer barrier for the corrosive species. However, for tests at pH 7.1, 6.6 and 6.0, the surface is either not fully covered with densely packed prism-shaped $FeCO_3$ crystals or it is covered by loose platelets of $FeCO_3$. It is difficult to imagine that such a layer can be a significant mass transfer barrier which reduces the corrosion rate. However, from Figure 4 it is clear that there is still corrosion protection in these cases. Furthermore in the test at pH7.1, the protection is as good as for the test at pH 7.8 while the surface layer does not seem to be nowhere as densely packed. How a seemingly incomplete corrosion product layer can still provide significant corrosion protection cannot be deduced from these SEM images.

Therefore, several cross section samples of the surface layer were prepared to further examine its characteristics. In order to get appreciable resolution, a TEM was used on a cross section sample produced by FIB. The corrosion product layer produced in the test at pH 7.1 was analyzed, as shown in Figure 6. Outlines of three $FeCO_3$ crystals can be recognized (seen in the top view as well), however, there is a continuous layer, approximately 2μm in thickness beneath them and no “bare” steel surface can be seen. A grazing incidence XRD measurement was made to obtain the phase identity information of this sample and is shown in Figure 7. Only $FeCO_3$ can be identified on the surface. Several line pattern EDS scans (Figure 8) were conducted to investigate the chemical composition at the boundary of the two large $FeCO_3$ crystals and at the interface between Fe and $FeCO_3$, in the hope of detecting any minor phases. The scan locations and directions are marked by red arrows and numbered in Figure 6 (b). There is no direct indication of any phases other than Fe and $FeCO_3$ existing on the surface.

Similar surface analyses have been applied to specimens from other tests. The cross-section and XRD results for the test at pH 6.0 are shown in Figure 9(a) and (b), respectively. A $FeCO_3$ layer is still seen to exist beneath the plate-shaped crystals at the surface. In this condition, a new phase, $Fe_2CO_3(OH)_2$, was also identified. For the test at pH 5.6 which has shown no corrosion protection, a cross-section and XRD analysis were also made, as shown in Figure 10 (a) and (b). No continuous $FeCO_3$ layer can be seen from the cross section, and the XRD indicates that iron is dominant. Trace amounts of $FeCO_3$ and $Fe_2CO_3(OH)_2$ were also identified.

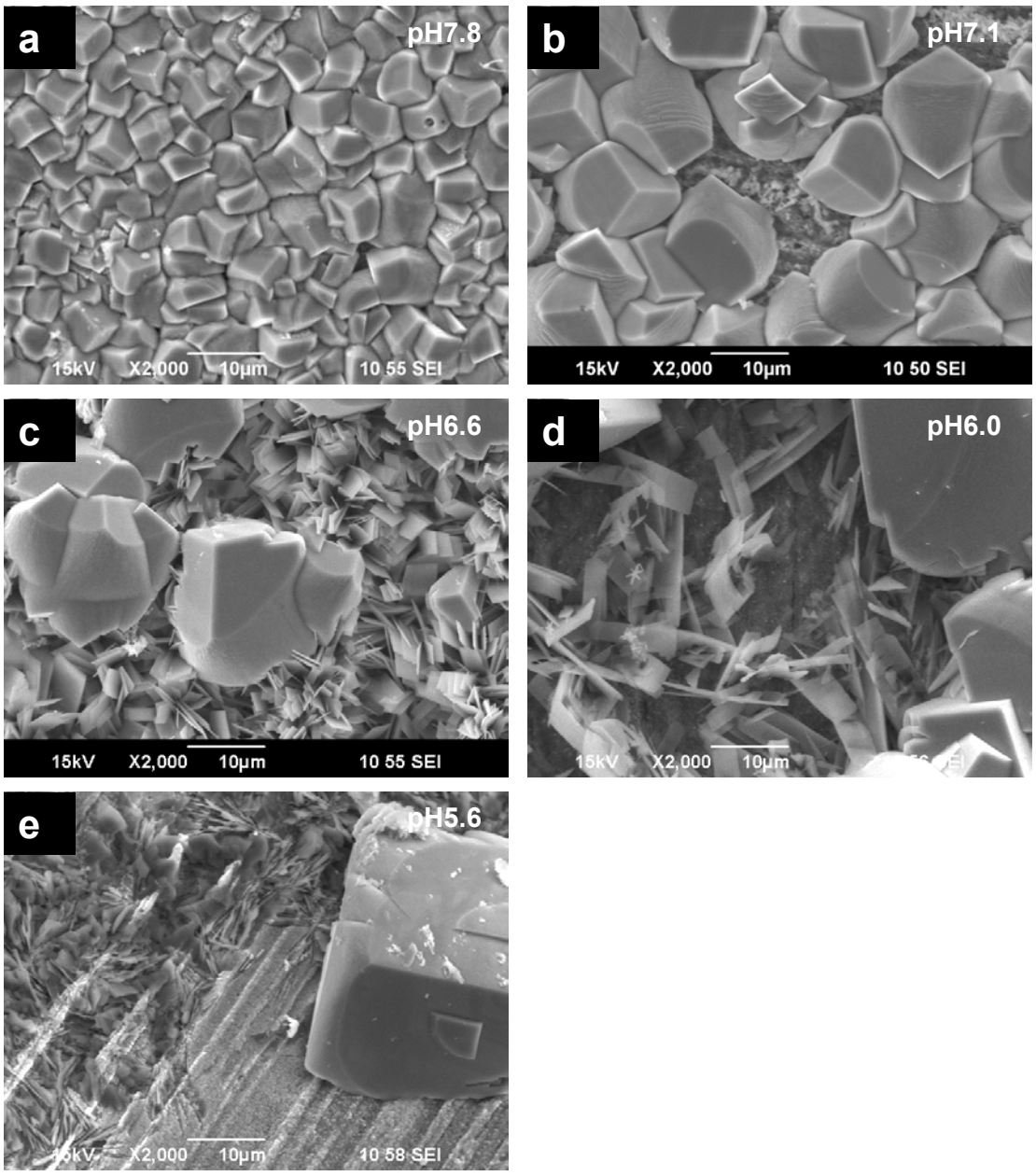

Figure 5: Top view SEM images taken at the end of tests at different pH (80°C, 0.53 bar (53 kPa) CO_2, 1 wt.% NaCl, stagnant): (a) pH 7.8; (b) pH 7.1; (c) pH 6.6, initial $C_{Fe^{2+}}$= 50 ppm; (d) pH 6.0, initial $C_{Fe^{2+}}$= 100 ppm; (e) pH 5.6, initial $C_{Fe^{2+}}$= 1000 ppm, second $C_{Fe^{2+}}$addition at the 13th day to 1400 ppm. For corresponding corrosion rate/potential images see Figure 4.

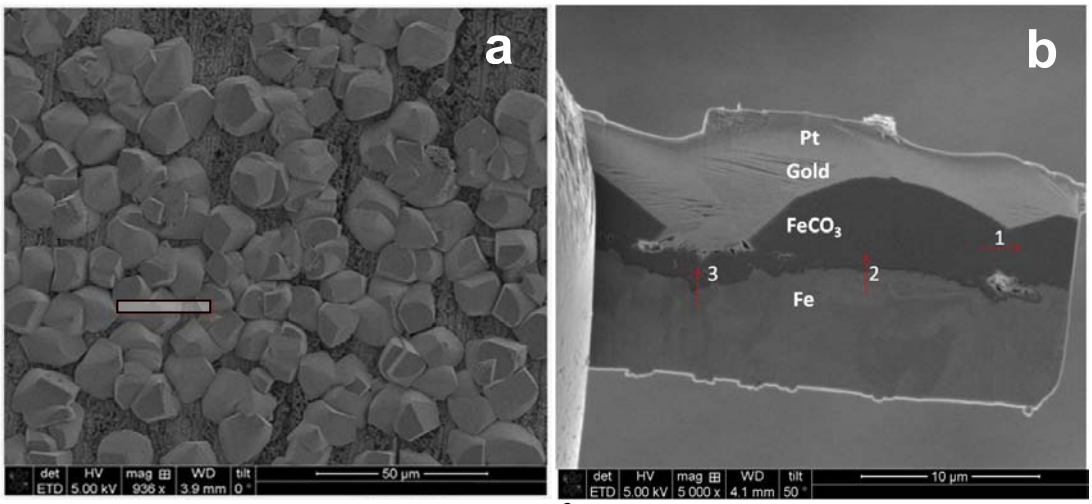

Figure 6: TEM images for test conditions of 80°C, 0.53 bar (53 kPa) CO_2, 1 wt.% NaCl, stagnant, pH 7.1, after 4 days: (a) top view of TEM sample denoting the cutting area; (b) side view of prepared TEM sample and locations of line EDS scans.

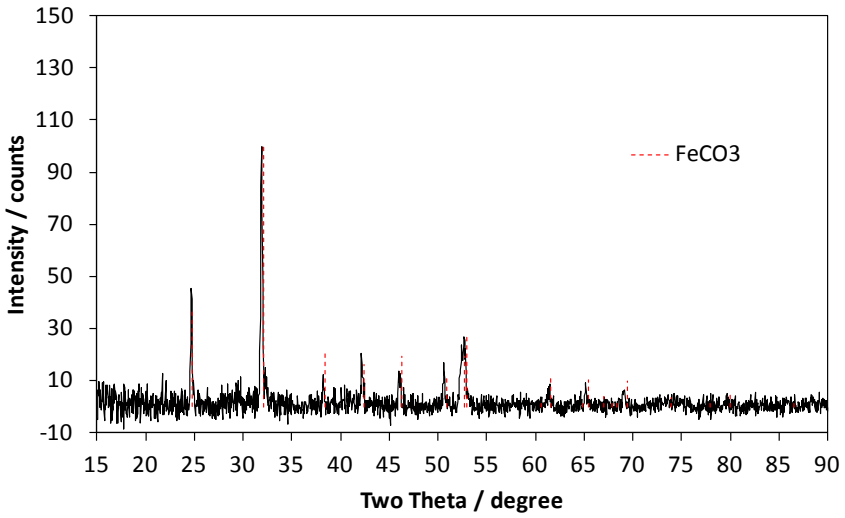

Figure 7: GIXRD pattern of X65 flat sample (80°C, 0.53 bar (530 kPa) CO_2, 1 wt.% NaCl, stagnant, pH 7.1, after 4 days).

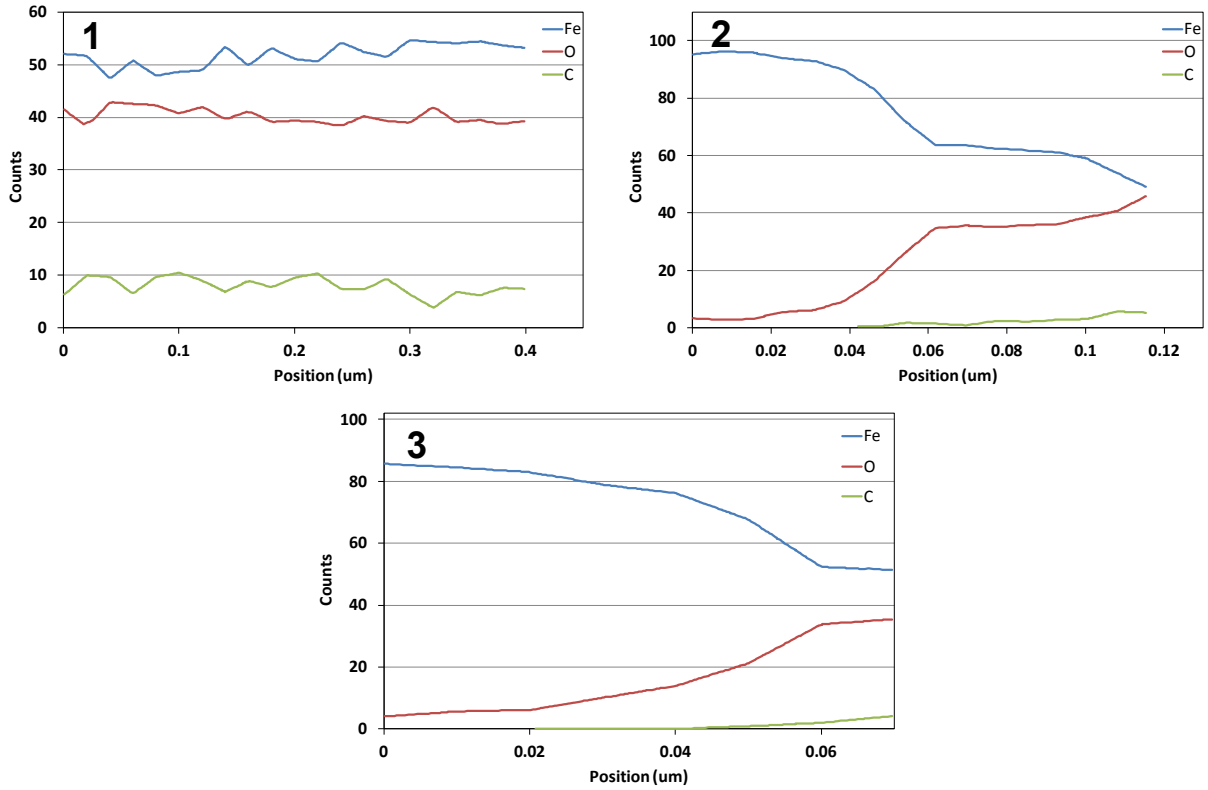

Figure 8: Line pattern EDS scan result of locations 1, 2, 3 shown in Figure 6.

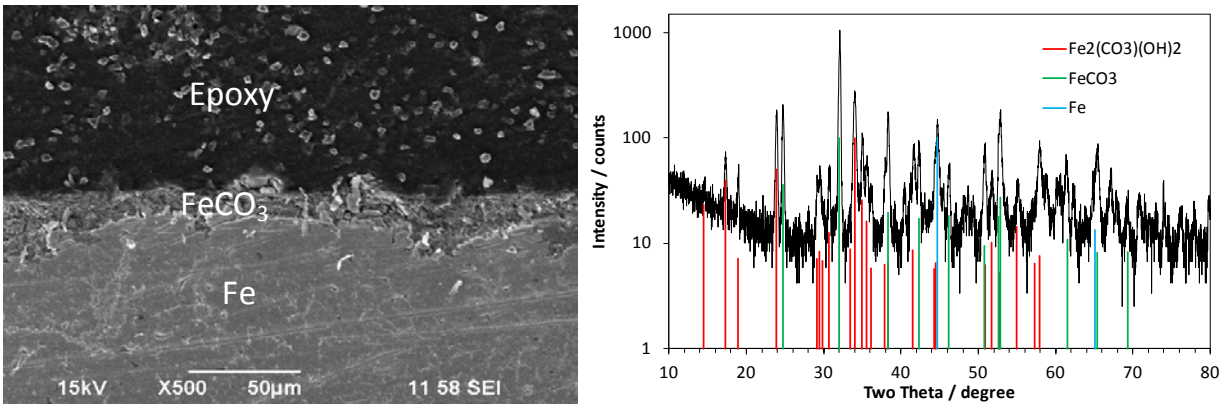

Figure 9: SEM cross section and XRD pattern of X65 sample (80°C, 0.53 bar (53 kPa) CO_2, 1 wt.% NaCl, stagnant, pH 6.0, initial $C_{Fe^{2+}}$ = 100 ppm, after 10 days).

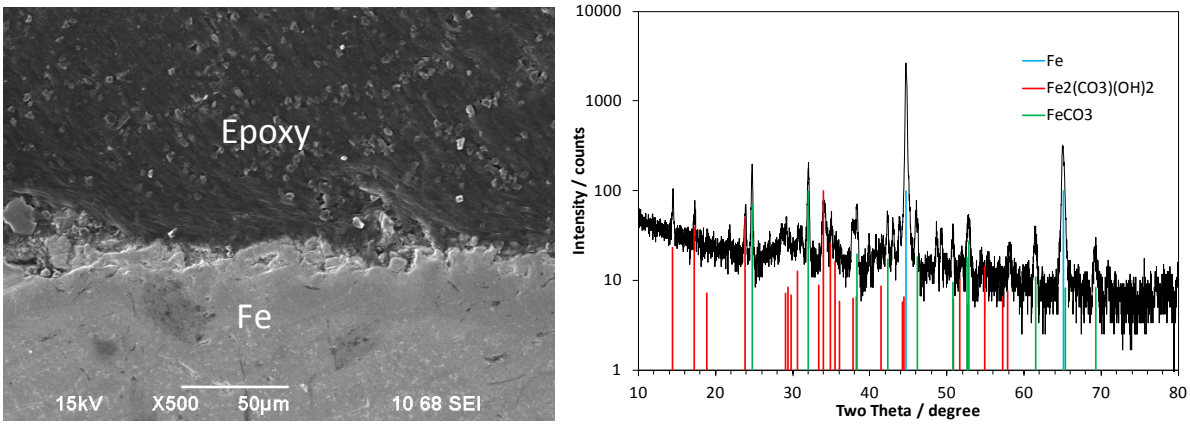

Figure 10: SEM cross section and XRD pattern of X65 sample. 80°C, 0.53 bar (530 kPa) CO_2, 1 wt.% NaCl, stagnant, pH 5.6, initial $C_{Fe^{2+}}$= 1000 ppm, after 22 days.

Discussion

Iron carbonate precipitation is seen when the saturation level of the solution is exceeded. This will more readily occur at the surface of the corroding steel where the concentration of ferrous ions $C_{Fe^{2+}}$ and the pH are both higher than in the bulk. A protective $FeCO_3$ layer formed in the present experiments at pH6 and above, however, this "threshold" pH is lower when the CO_2 partial pressure is higher and at higher temperature.

The protectiveness of the $FeCO_3$ layer is usually associated with its thickness and porosity, as seen in the SEM images. It is common to assume that the protectiveness is due to the mass transfer resistance which a dense and thick $FeCO_3$ layer offers against inward diffusion of corrosive species. The present experiments have shown that this is only partially correct. For example, good protection was also seen in experiments where the $FeCO_3$ layer was not dense or thick. Furthermore, the open circuit potential increased when protective $FeCO_3$ layer formed which is opposite of what is expected when a cathodic reaction is slowed down due to a diffusion limitation.

It was discovered that a thin (~ 1um) adherent inner layer forms, which seems to be the key to corrosion protection. In the experiments conducted here this layer was found to be $FeCO_3$. In other studies at higher pH and temperature, magnetite, Fe_3O_4, was also found in this inner layer. Regardless, the protectiveness of this thin layer seemed to be associated with its adherence to the surface as much as it was related to its composition. Given the rise in open circuit potential seen when protective corrosion product layers form in CO_2 corrosion, it was deduced that the protection comes from the retardation of the anodic reaction more than the cathodic reaction. Therefore, it is speculated that the thin adherent corrosion product layer covers/blocks large portions of the steel surface thereby directly retarding anodic dissolution of iron, which manifests itself as a rise in open circuit potential. The simultaneous reduction of the corrosion rate and increase in the open circuit potential are similar to *passivity*, however, this behavior is different. The inner layer that forms is still "macroscopic" (visible in SEM and TEM) and the effect is reversible, *i.e.*, the layer is readily removed in undersaturated (typically more acidic) solutions along with the passive-like protection. Therefore the term that is used is *pseudo-passivity*.

There is a role of mass transfer in this scenario. The "outer" more porous $FeCO_3$ layer which forms first does retard the diffusion of corrosive species to the surface but also the diffusion of ferrous ions away from it. This leads to a very different water chemistry at the corroding steel surface when compared to the bulk, where the ferrous ion concentration is much higher and so is the pH, both facilitating formation of the inner more adherent and more protective thin layer.

CONCLUSIONS

The pH effect on protective corrosion product layer formation in mild steel CO_2 corrosion has been studied. Tests at 80°C, with pH ranging from 7.8 to 5.6, have been conducted. Several conclusions can be drawn from the results and discussion of this work:

- In the pH range from 7.8 to 6.0 (at 80°C, 0.53 bar CO_2), a protective pseudo-passive layer was observed. This layer significantly lowered the corrosion rate with a noticeable open circuit potential increase.
- The surface analyses of this pseudo-passive layer revealed that it was made from $FeCO_3$, that it was thin (~ 1um) and very well attached to the steel surface and worked primarily by directly blocking the anodic iron dissolution reaction.
- The mass transfer resistance offered by the much thicker outer $FeCO_3$ crystalline layer was not a direct contributor to corrosion protection, as usually assumed. Its role was primarily to create conditions at the steel surface (high ferrous ion concentration and pH) which are favorable for formation of the inner pseudo-passive layer.
- No pseudo-passive layer could be formed at pH 5.6 at 80°C and 0.53 bar CO_2.
- A threshold pH of 6.0 is needed to get a protective corrosion product layer, this would be lower at higher partial pressure of CO_2 and at higher temperature.

ACKNOWLEDGEMENTS

This paper represents an abridged version of the first author's thesis, which was submitted to the Ohio University in partial fulfillment of the requirements for the degree of Master of Science. The work and revision were conducted under the guidance of Dr. Srdjan Nešić of the Department of Chemical and Biomolecular Engineering at Ohio University. The work was financially sponsored from the Corrosion Center Joint Industry Project at Ohio University.

REFERENCES

1. J. Han, B. N. Brown and S. Nešić, "Investigation of the galvanic mechanism for localized carbon dioxide corrosion propagation using the artificial pit technique," *Corrosion,* vol. 66, pp. 095003-1 – 095003-12, 2010.
2. C. De waard and D. E. Milliams, "Prediction of carbonic acid corrosion in natural gas pipelines." in *1st International Conference on the Internal and External Protection of Pipes,* University of Durham, UK, 1975.
3. L. G. S. Gray, B. G. Anderson, M. J. Danysh and P. R. Tremaine, "Mechanisms of carbon steel corrosion in brines containing dissolved carbon dioxide at pH 4," in *NACE Corrosion 89,* New Orleans Convention Center, New Orleans, Louisiana, USA, 1989.
4. L. G. S. Gray, B. G. Anderson, M. J. Danysh and P. R. Tremaine, "Effect of pH and temperature on the mechanism of carbon steel corrosion by aqueous carbon dioxide," in *NACE Corrosion 90,* Bally's Hotel, Las Vegas, Nevada, USA, 1990.
5. S. Nešić, J. Postlethwaite and S. Olsen, "An Electrochemical Model for Prediction of Corrosion of Mild Steel in Aqueous Carbon Dioxide Solutions," *Corrosion (Houston),* vol. 52, pp. 280-294, 1996.
6. S. Nešić, M. Nordsveen, R. Nyborg and A. Stangeland, "A mechanistic model for carbon dioxide corrosion of mild steel in the presence of protective iron carbonate films - Part 2: A numerical experiment," *Corrosion,* vol. 59, pp. 489-497, 2003.
7. S. Nešić and W. Sun, "Corrosion in acid gas solutions," in *Shreir's Corrosion*, Tony J.A. Richardson, Ed. Oxford: Elsevier, 2010, pp. 1270-1298.
8. Y. K. Kharaka and Geological Survey, *SOLMINEQ.88, a Computer Program for Geochemical Modeling of Water-Rock Interactions.* Menlo Park, Calif.: Dept. of the Interior, U.S. Geological Survey, 1989.
9. J. E. Oddo and M. B. Tomson, "Simplified calculation of $CaCO_3$ saturation at high temperatures and pressures in brine solutions." *Journal of Petroleum Technology,* vol. 34, pp. 1583-1590, 1982.
10. D. A. Palmer and R. Van Eldik, "The chemistry of metal carbonato and carbon dioxide complexes," *Chem. Rev.,* vol. 83, pp. 651-731, 1983.
11. W. Sun, S. Nešić and R. C. Woollam, "The effect of temperature and ionic strength on iron carbonate ($FeCO_3$) solubility limit," *Corros. Sci.,* vol. 51, pp. 1273-1276, 2009.
12. J. Han, D. Young, H. Colijn, A. Tripathi and S. Nešić, "Chemistry and Structure of the Passive Film on Mild Steel in CO_2 Corrosion Environments," *Ind Eng Chem Res,* vol. 48, pp. 6296-6302, 2009.
13. G. Schmitt and M. Hörstemeier, "Fundamental aspects of CO_2 metal loss corrosion - Part II: Influence of different parameters on CO_2 corrosion mechanisms," *NACE - International Corrosion Conference Series,* pp. 06112-1 – 06112-26, 2006.